ChemComm

Heterobimetallic Single-Source Precursor Enables Layered Oxide Cathode for Sodium-Ion Battery

Journal:	*ChemComm*
Manuscript ID	CC-COM-05-2018-004205.R2
Article Type:	Communication

Chem Comm

COMMUNICATION

Heterobimetallic Single-Source Precursor Enables Layered Oxide Cathode for Sodium-Ion Battery

Received 00th January 2017,
Accepted 00th January 2017

DOI: 10.1039/x0xx00000x

www.rsc.org/

Maofan Li,[a] Kai Yang,[a] Jiajie Liu,[a] Xiaobing Hu,[b] Defei Kong,[a] Tongchao Liu,[a] Mingjian Zhang,*[ac] and Feng Pan*[a]

The single-source precursor $NaCo(acac)_3$ (acac=acetylacetone) for the layered oxide cathodes of sodium-ion batteries (SIBs) is reported here. It features a 1D chain structure, and is prepared in nearly quantitative yield employing commercially available reagents. The complex is stable in open air and tends to dissolve in various strongly polar solvents, including H_2O and methanol. The phase-pure layered oxide cathode material P2-Na_xCoO_2 for SIBs is obtained through calcining the complex, and exhibits an excellent rate capability, even superior than the recently-reported P2-Na_xCoO_2 microspheres. More analogue complexs could be obtained through cationic replacement for the synthesis of other high-performance layered metal oxides for SIBs.

Since the first commercialization of lithium-ion batteries(LIBs) based on $LiCoO_2$ in 1991 by Sony, LIBs have made great progress and are widely used in human life such as laptops, mobiles, electronic vehicles, etc. in the past 27 years, owing to the low cost and high energy density.[1-4] As LIBs expand their application from portable electronics to electric vehicles and grid storages, a great concern arises about the widespread availability and rising price due to the low abundance of lithium resources on earth. As a good alternative to LIBs, sodium-ion batteries(SIBs) with lower cost have attracted increasing attention because of the super high abundance of Na,[5-8] and its redox potential (-2.71 V vs. SHE) close to lithium (-3.03V Vs. SHE).[9] In fact, LIBs and SIBs were studied almost simultaneously.[10-13] In 1980, when layered $LiCoO_2$ was first reported as a cathode material for LIBs, the electrochemical activity of layered Na_xCoO_2 was also confirmed for SIBs.[14, 15] In the viewpoint of the high similarity of the physical and chemical properties of lithium and sodium, Na_xCoO_2 has always been considered as a promising cathode material for SIBs since the great success of $LiCoO_2$ for LIBs. However, the practical application of Na_xCoO_2 is hindered by the poor rate capability and cycling performance. Many efforts have been devoted to understanding and fixing this concern. The *in situ* X-ray diffraction (XRD) studies demonstrated that, a series of abrupt phase transformations happened during Na^+ extraction/insertion due to the great sensitivity of Na^+ ordering to the Na^+ content in layered structure.[16, 17] Several effective approaches are developed to improve its cycling stability and rate capability, such as doping or substitution of other cations through suppressing the Na^+ ordering (e.g. Ca^{2+}, Ti^{4+}, Cr^{3+} and $Mn^{3+/4+}$),[18-23] and the constructing of special microscopic architectures (e.g. microspheres).[24] All these efforts are mainly confined in the solid-state (SS) synthesis of Na_xCoO_2. Similar with the case in Li-ion batteries, the electrochemical performance of layered cathodes for Na-ion batteries is also greatly affected by the phase purity, the stoichiometry and distribution of constituent elements, the morphology uniformity and the properties of the particle surface.[25, 26] Lots of efforts have been devoted to improving the electrochemical performance through elemental substitution and doping,[27-30] surface modification,[31, 32] and etc., but little work is reported about tuning the uniformity of elemental distribution and the particle morphology partially due to the difficulty and rarity of developing new synthesis methods.

For so long, the SS method is always the main-stream route for the synthesis of Na_xCoO_2, wherein firstly mixing Na source (Na_2CO_3, NaOAc, and etc..) and Co source (Co_3O_4, $CoCO_3$, $Co(OH)_2$ and etc..) by grinding or ball milling, then performing calcination.[17, 33-35] It naturally brings with some concerns, such as the inhomogeneity of elemental distribution, the nonuniformity of morphologies, and the dirty surface of individual particles, which are detrimental to the final electrochemical performance of products. To develop new synthesis routes is essential to provide opportunities to solve these issues, thereby enhance the electrochemical performance. As an emerging method, the single-source precursor (SP) method, known as combining all the involving metal elements in one single compound with proper ratios, have delivered enhanced electrochemical performance in preparing cathode materials for LIBs, due to the great uniformity of elemental distribution and fancy morphologies. Layered $LiCoO_2$, spinel $LiMn_2O_4$ and layered $LiFeO_2$ has been reported by Dikarev group.[36-38] Our group also reported multiple layered oxides for Li-ion batteries through the SP method.[39] Nevertheless, this method has never been extended into the synthesis of layered oxides cathode materials for SIBs except for the nonoxide case $NaMF_3$ (M=Mn^{2+}, Fe^{2+}, Co^{2+} and Ni^{2+}).[40]

[a] *School of Advanced Materials, Peking University, Peking University Shenzhen Graduate School, Shenzhen 518055, China.*
[b] *Condensed Matter Physics and Materials Science Department, Brookhaven National Laboratory, Upton, New York 11973, USA.*
[c] *Sustainable Energy Technologies Department, Brookhaven National Laboratory, Upton, New York 11973, USA.*
E-mail: zhangmj@pkusz.edu.cn，panfeng@pkusz.edu.cn
Electronic Supplementary Information (ESI) available. See DOI: 10.1039/x0xx00000x

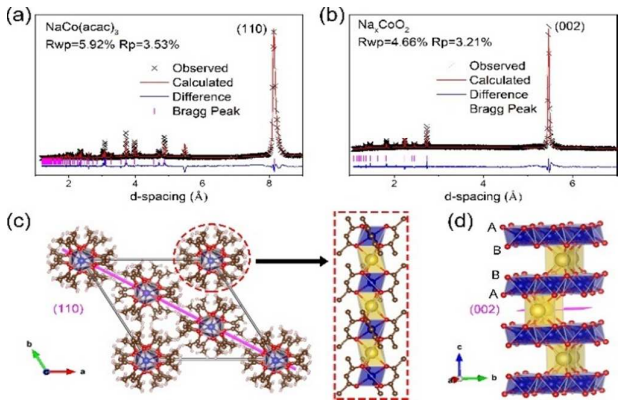

Figure 1. Experimental and refined XRD patterns of $NaCo(acac)_3$ (a) and Na_xCoO_2 (b); the structural sketch maps of $NaCo(acac)_3$ (c) and Na_xCoO_2 (d).

In this work, a carbonyl-bridged single-source precursor $NaCo(acac)_3$ (acac=acetylacetone) featured 1D chain structure, was successfully designed and applied to achieve the layered oxide cathode materials P2-Na_xCoO_2 here. In comparison with the conventional SS method, Na_xCoO_2 obtained by this SP method exhibited enhanced electrochemical performance, especially the superior rate capability (70 mAh g^{-1} at the current density of 2000 mA g^{-1}), which is even superior than the recently-reported spherical Na_xCoO_2 (64 mAh g^{-1} at the current density of 2000 mA g^{-1}). It could be ascribed to the great uniformity of elemental distribution at the nanometer level. This method opens a new avenue to prepare high-performance layered metal oxide cathodes for SIBs.

The heterometallic precursor $NaCo(acac)_3$ was synthesized by the solution reflux method (Figure S1). Initially the below reaction was followed:

$$3\ Na(acac) + CoCl_2 \rightarrow NaCo(acac)_3 + 2\ NaCl \quad (1)$$

While this reaction affords two products $NaCo(acac)_3$ and NaCl, which are both hard to dissolve in ethanol, and readily to dissolve in strongly polar solvents, such as H_2O and methanol. It is hard to find an appropriate solvent to achieve pure $NaCo(acac)_3$. One method to solve this issue is utilizing the sublimation character of $NaCo(acac)_3$ at temperatures below the decomposition temperature to purify it (Figure S5). The other method is using commercially available reagent $Co(acac)_2$ to replace the $CoCl_2$ to obtain pure $NaCo(acac)_3$ without any additional purification by following Reaction (2).

$$Na(acac) + Co(acac)_2 \rightarrow NaCo(acac)_3 \quad (2)$$

As shown in Figure S2, the pink powder of $NaCo(acac)_3$ can be readily collected in nearly quantitative yield within several hours at a low temperature (55 ℃), making it attractive for the large-scale application. As shown in Figure 1a, the purity has been confirmed by comparing the X-ray powder diffraction (XRD) pattern with the calculated one from the single crystal data (Table S2-S5). The product was observed to be stable in ambient conditions and can be handled without using a glovebox for further studies.

The single crystals, presenting the prism shape with orange color (Figure S3), were grown by the vapor diffusion method (see supporting Information). X-ray diffraction studies revealed the crystal structure of $NaCo(acac)_3$ in Figure 1c. It crystalized in space group *R*-3*c*,[41] same with its analogue $LiCo(acac)_3$.[38] As we can see, it was constructed by a lot of parallel-aligned 1D chains along the c axis, which were consisted by the alternately-connected Na^+ and $[Co(acac)_3]$ uints. Thereinto, Co^{2+} cations exhibit octahedra geometry of six oxygens from three chelating acac molecules, and Na+ ions present trigonal prism geometry by six oxygen atoms from six acac molecules.

Na_xCoO_2 was obtained by calcining $NaCo(acac)_3$ at 850 ℃ in air. The powder XRD pattern was illustrated in Figure 1b.

The Rietveld refinement were performed by using P2-type $NaCoO_2$ with space group $P6_3/mmc$ (ICSD 246585), respectively. The detailed refinement parameters for XRD patterns were deposited in Table S5. As shown in Figure 1d, P2-Na_xCoO_2 presents an AB BA oxygen packing structure with cobalt ions in octahedral sites and Na^+ ions in octahedral or prismatic sites. Accordingly, the NaO_6 octahedra and CoO_6 octahedra in the precursor are the basic structural unit to produce the layered oxides Na_xCoO_2. The similarity of basic structural units ensures the successful phase transformation from the precursor $NaCo(acac)_3$ to P2-Na_xCoO_2.

The morphologies of the precursor $NaCo(acac)_3$ and the product P2-Na_xCoO_2 were investigated by SEM and TEM characterization. As shown in Figure 2a, the precursor presented a uniform prism shape, with length about 3–5 μm and width about 100–200 nm. This shape was well consistent with their hexagonal crystal structure shown in Figure 1c, because the crystals preferred to grow up along the c axis by extending the 1D chain. The product Na_xCoO_2 presented the uniform hexagonal thick-plate shape with diameter about 5–10 μm and thickness about 2–4 μm in Figure 2b. Figure 2c presented the high resolution TEM. The indexing of (002) crystallographic planes indicated that, the thick plate was constructed by parallelly-stacking lots of single thin slabs along the c axis, which might be beneficial to Na^+ fast de/intercalation to enhance the rate capability. As shown in Figure 2d, the selected-area electron diffraction (SEAD) revealed the existence of superlattices in Na_xCoO_2 as an intrinsic bulk characteristic. This superlattice structure indicated Na^+/vacancy ordering between CoO_2 layers, which has been reported to take place at a certain sodium content.[42-46] By comparing the TEM images in Figure S8, a much cleaner surface was obtained for Na_xCoO_2 prepared by single-source precursor method than that

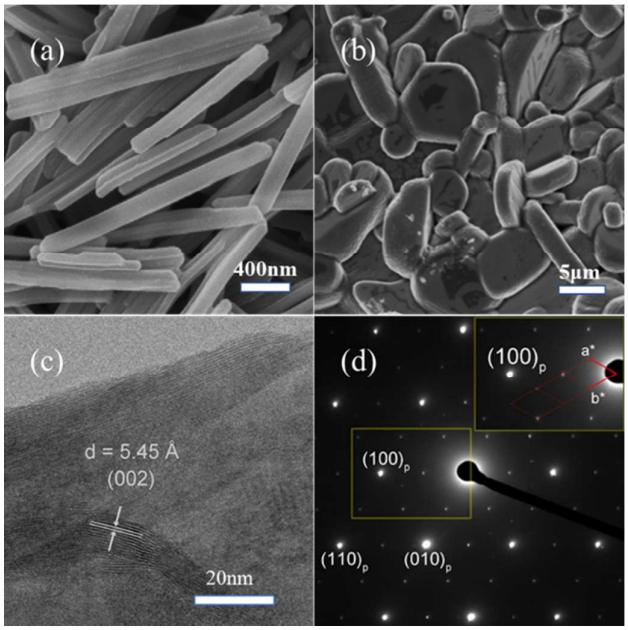

Figure 2. SEM images of $NaCo(acac)_3$ (a) and Na_xCoO_2 (b); (e) High resolution TEM image of Na_xCoO_2; (f) Selected-area electron diffraction (SAED) pattern of Na_xCoO_2.

prepared by the solid-state method, which may be benefit to the fast Na^+ de/intercalation during the electrochemical tests.

In addition, the chemical compositions were measured by ICP-AES (Table S1). The molar ratio of Na and Co in $NaCo(acac)_3$ is 1.012:1.000. After calcination, the molar ratio in Na_xCoO_2 decreased to 0.772:1.000, indicating a 23% Na loss during the sintering. This is in agreement with the earlier report,[35] wherein an excess amount (20%) of sodium source has been added to compensate for the sodium loss during calcination. Combining ICP-AES results (Table S1) with TGA results (Figure S4), Na loss during calcination mainly occurs at around 600 □, which corresponds to a small weight loss of 2.44% at around 600 □ (marked with a red dashed rectangle in Figure S4).

The entire morphology evolution process from $NaCo(acac)_3$ to P2-Na_xCoO_2 was tracked by SEM images in Figure 3a. From RT to 200 □, the prism shape of $NaCo(acac)_3$ was basically preserved, but every individual prism decomposed into lots of nanoparticles, which was identified as spinel Co_3O_4 and some kind of unknown Na source by XRD pattern in Figure S6. The high uniformity in the mixture of Na source and Co source at the nanometer level was demonstrated here. This kind of superiority, which usually could not be achieved by grinding or ball-milling in the traditional SS method, provides the base for the superiority of the SP method. As the temperature was elevated to 400 □, the prism shape completely disappeared, and nanosized particles merged and grew into sub-micrometer particles with size around 100–500 nm. Further up to 600 □, the particle size was increased to 500–1000 nm, and the phase has completely transformed to P3-Na_xCoO_2. Finally, the layered P2-Na_xCoO_2 with high crystallinity and larger particle size was obtained at 850 □, presenting the regular hexagonal plate shape. The multi-step phase transition process involving P3 intermediate phase was similar with the traditional SS method.[47, 48] Correspondingly, the multiply-step thermal decomposition process during the calcination was also observed by the TGA/DSC curves of $NaCo(acac)_3$ in Figure S4.

Based on the morphology evolution process, it is easy to understand how the atomic-level uniformity of elemental distribution (Na and Co) in the single-source precursor $NaCo(acac)_3$ lead to the nanoscale-level uniformity of elemental distribution in Na_xCoO_2. The elemental uniformity of $NaCo(acac)_3$ and Na_xCoO_2 has been further confirmed by the SEM and TEM EDX elemental mappings (Figure S7 and 3b).

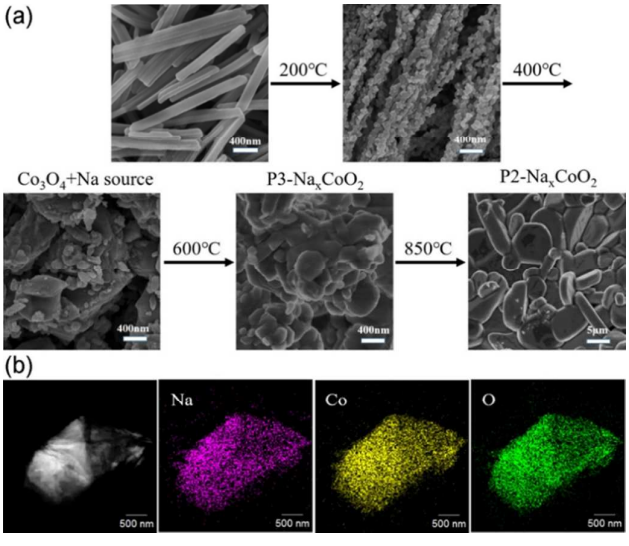

Figure 3. (a) The SEM images for $NaCo(acac)_3$ calcined at different temperatures to show the morphology evolution from the precursor $NaCo(acac)_3$ to the product Na_xCoO_2; (b) the TEM EDX mapping for single particle of Na_xCoO_2.

Finally, Na_xCoO_2 prepared by the SP and SS methods were both assembled into half cells to test their electrode performance. The galvanostatic charge and discharge performance has been tested at various current densities (10, 20, 50, 100, 200, 500, 1000, and 2000 mA g^{-1}) as shown in Figure 4a for determining the rate tolerance of the materials. Five cycles were performed at each current density and finally returned to 100 mA g^{-1}. At 10, 20, 50, 100, 200, 500, 1000, 2000, and 100mA g^{-1}, the average discharge capacities for five cycles are 101.7, 105.3, 105.9, 104.0, 101.1, 93.6, 82.7, 69.9, and 100.8 mA h g^{-1} for Na_xCoO_2 prepared by the SP method, obviously higher than the corresponding values for Na_xCoO_2 prepared by the SS method. The cells both showed higher capacities when the current density increased from 10 to 20 and 50 mA g^{-1}, a similar phenomenon was previously reported in lithium ion battery cathode materials, and may be related with a activation process of P2-Na_xCoO_2 during the first several cycles.[49, 50] Figure 4b depicts the charge/discharge profiles of Na_xCoO_2 at different current densities, which were extracted from the third cycle of every five cycles. At 10 mA g^{-1}, anodic and cathodic plateaus are clearly visible at 4.00, 3.70, 3.31, 3.19, 3.00, 2.73, 2.67, 2.62, 2.55 and 3.93, 3.62, 3.20, 3.13, 2.90, 2.60, 2.55, 2.47, 2.33V respectively. These plateaus are quite consistent with the redox couples observed in cyclic voltammetry (CV) studies at 0.3 mV s^{-1} in Figure S10. As shown in Table S7, Excellent rate performance reported here are better than all those Na_xCoO_2 prepared by the SS method in earlier reports,[33-35] even superior than the recently-reported spherical Na_xCoO_2 (64 mAh g^{-1} at the current density of 2000 mA g^{-1}).[24] The cycling stability for Na_xCoO_2 prepared by the SP method was tested with current densities of 100, 500 and 1000 mA g^{-1}. Figure 4c shows very good capacity retentions, 90%, 96%, and 95% after 50 cycles, respectively. The charge/discharge profiles in Figure 4d show a ladder-like behavior, which is also supported by earlier reports.[18-20, 34] Charge/discharge capacities of 1, 10 and 50 cycles are 110.1/104.6, 105.3/103.1 and 95.8/94.2 mA h g^{-1} respectively. According to the previous reports, the cycling stability, could be further improved by doping other elements, such as Ca^{2+} and Ti^{4+}.[18, 34]

In summary, the heterometallic single-source precursor

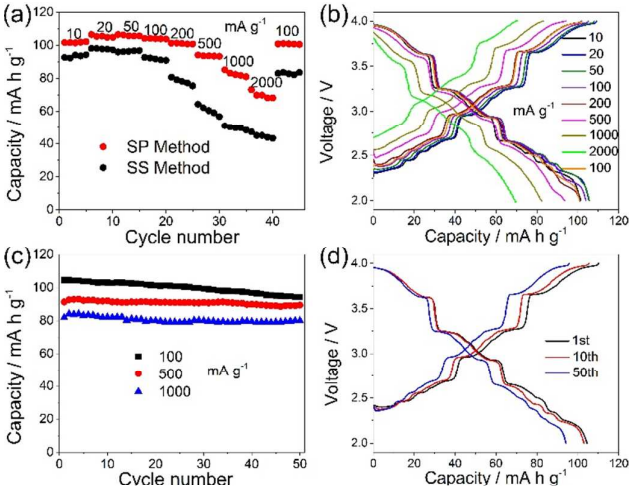

Figure 4. Electrochemical performance of Na_xCoO_2. Rate performance of P2-Na_xCoO_2 prepared by the SP and SS methods (a); charge and discharge profiles with different current densities for P2-Na_xCoO_2 prepared by the SP method (b); cycling performance with current densities of 100, 500 and 1000 mA g^{-1} (c); and charge and discharge profiles at selected cycles with a current density of 100 mA g^{-1} for P2-Na_xCoO_2 prepared by the SP method (d).

$NaCo(acac)_3$ was successfully designed and prepared for the synthesis of P2-Na_xCoO_2 for SIBs. When acting as a cathode for SIBs, it exhibited excellent electrochemical performance, especially the superior rate capability, which could be ascribed to the great uniformity of particle morphology, and the clean particle surface. It provides a unique and valuable approach to prepare high performance electrode materials for SIBs. More layered Na-ion cathode materials, such as P2-$Na_{0.7}MnO_2$, O3-$NaFeO_2$ and $Na_x(Ni/Co/Mn)O_2$, even including layered K-ion materials, are expected to be prepared by this method.

Conflicts of interest

There are no conflicts to declare.

Acknowledgements

This work was supported by the Guangdong innovative team program (2013N080), the peacock plan (KYPT20141016105435850), Shenzhen Science and Technology Research Grant (JCYJ20151015162256516, JCYJ20150729111733470), Chinese postdoctoral science foundation (2015M570882, 2015M570894), the International Postdoctoral Exchange Fellowship Program (No. 53 Document of OCPC, 2016), the U. S. Department of Energy (DOE) Office of Energy Efficiency and Renewable Energy under the Advanced Battery Materials Research (BMR) program (DE-SC0012704).

Notes and references

1. M. S. Whittingham, *Chem. Rev.*, 2014, **114**, 11414-11443.
2. M. Armand and J. M. Tarascon, *Nature*, 2008, **451**, 652-657.
3. M. M. Thackeray, C. Wolverton and E. D. Isaacs, *Energy Environ. Sci.*, 2012, **5**, 7854-7863.
4. M. D. Radin, S. Hy, M. Sina, C. C. Fang, H. D. Liu, J. Vinckeviciute, M. H. Zhang, M. S. Whittingham, Y. S. Meng and A. Van der Ven, *Adv. Energy Mater.*, 2017, **7**, 1602888.
5. V. Palomares, M. Casas-Cabanas, E. Castillo-Martinez, M. H. Han and T. Rojo, *Energy Environ. Sci.*, 2013, **6**, 2312-2337.
6. V. Palomares, P. Serras, I. Villaluenga, K. B. Hueso, J. Carretero-Gonzalez and T. Rojo, *Energy Environ. Sci.*, 2012, **5**, 5884-5901.
7. S. W. Kim, D. H. Seo, X. H. Ma, G. Ceder and K. Kang, *Adv. Energy Mater.*, 2012, **2**, 710-721.
8. N. Yabuuchi, K. Kubota, M. Dahbi and S. Komaba, *Chem. Rev.*, 2014, **114**, 11636-11682.
9. S. P. Ong, V. L. Chevrier, G. Hautier, A. Jain, C. Moore, S. Kim, X. H. Ma and G. Ceder, *Energy Environ. Sci.*, 2011, **4**, 3680-3688.
10. M. S. Whittingham, *Prog. Solid State Chem.*, 1978, **12**, 41-99.
11. G. H. Newman and L. P. Klemann, *J. Electrochem. Soc.*, 1980, **127**, 2097-2099.
12. Y. J. Fang, X. Y. Yu and X. W. Lou, *Adv. Mater.*, 2018, **30**, 1706668.
13. P. L. He, Y. J. Fang, X. Y. Yu and X. W. D. Lou, *Angew. Chem. Int. Ed.*, 2017, **56**, 12202-12205.
14. K. Mizushima, P. C. Jones, P. J. Wiseman and J. B. Goodenough, *Mater. Res. Bull.*, 1980, **15**, 783-789.
15. C. Delmas, J. J. Braconnier, C. Fouassier and P. Hagenmuller, *Solid State Ionics*, 1981, **3-4**, 165-169.
16. M. Roger, D. J. P. Morris, D. A. Tennant, M. J. Gutmann, J. P. Goff, J. U. Hoffmann, R. Feyerherm, E. Dudzik, D. Prabhakaran, A. T. Boothroyd, N. Shannon, B. Lake and P. P. Deen, *Nature*, 2007, **445**, 631-634.
17. R. Berthelot, D. Carlier and C. Delmas, *Nat. Mater.*, 2011, **10**, 74-80.
18. S. M. Kang, J. H. Park, A. Jin, Y. H. Jung, J. Mun and Y. E. Sung, *ACS Appl. Mater. Interfaces*, 2018, **10**, 3562-3570.
19. Y. S. Wang, R. J. Xiao, Y. S. Hu, M. Avdeev and L. Q. Chen, *Nat. Commun.*, 2015, **6**, 6945.
20. N. Sabi, A. Sarapulova, S. Indris, H. Ehrenberg, J. Alami and I. Saadoune, *ACS Appl. Mater. Interfaces*, 2017, **9**, 37778-37785.
21. G. F. Gao, D. Tie, H. Ma, H. J. Yu, S. S. Shi, B. Wang, S. M. Xu, L. L. Wang and Y. F. Zhao, *J. Mater. Chem. A*, 2018, **6**, 6675-6684.
22. J. Y. Hwang, S. T. Myung, J. U. Choi, C. S. Yoon, H. Yashiro and Y. K. Sun, *J. Mater. Chem. A*, 2017, **5**, 23671-23680.
23. H. Park, J. Kwon, H. Choi, T. Song and U. Paik, *Sci. Adv.*, 2017, **3**, e1700509.
24. Y. J. Fang, X. Y. Yu and X. W. Lou, *Angew. Chem. Int. Ed.*, 2017, **56**, 5801-5805.
25. P. F. Wang, Y. You, Y. X. Yin and Y. G. Guo, *Adv. Energy Mater.*, 2018, **8**.
26. Y. You and A. Manthiram, *Adv. Energy Mater.*, 2018, **8**, 1701785.
27. D. Buchholz, C. Vaalma, L. G. Chagas and S. Passerini, *J. Power Sources*, 2015, **282**, 581-585.
28. Z. Y. Li, H. B. Wang, D. F. Chen, K. Sun, W. Y. Yang, J. B. Yang, X. F. Liu and S. B. Han, *ChemSusChem*, 2018, **11**, 1223-1231.
29. C. Zhang, R. Gao, L. R. Zheng, Y. M. Hao and X. F. Liu, *ACS Appl. Mater. Interfaces*, 2018, **10**, 10819-10827.
30. Y. You, S. O. Kim and A. Manthiram, *Adv. Energy Mater.*, 2017, **7**.
31. J. Zhang and D. Y. W. Yu, *J. Power Sources*, 2018, **391**, 106-112.
32. L. Q. Mu, M. M. Rahman, Y. Zhang, X. Feng, X. W. Du, D. Nordlund and F. Lin, *J. Mater. Chem. A*, 2018, **6**, 2758-2766.
33. J. J. Ding, Y. N. Zhou, Q. Sun, X. Q. Yu, X. Q. Yang and Z. W. Fu, *Electrochim. Acta*, 2013, **87**, 388-393.
34. S. C. Han, H. Lim, J. Jeong, D. Ahn, W. B. Park, K. S. Sohn and M. Pyo, *J. Power Sources*, 2015, **277**, 9-16.
35. B. V. R. Reddy, R. Ravikumar, C. Nithya and S. Gopukumar, *J. Mater. Chem. A*, 2015, **3**, 18059-18063.
36. A. Navulla, L. Huynh, Z. Wei, A. S. Filatov and E. V. Dikarev, *J. Am. Chem. Soc.*, 2012, **134**, 5762-5765.
37. H. X. Han, Z. Wei, M. C. Barry, A. S. Filatov and E. V. Dikarev, *Dalton Trans.*, 2017, **46**, 5644-5649.
38. Z. Wei, H. X. Han, A. S. Filatov and E. V. Dikarev, *Chem. Sci.*, 2014, **5**, 813-818.
39. M. F. Li, J. J. Liu, T. C. Liu, M. J. Zhang and F. Pan, *Chem. Commun.*, 2018, **54**, 1331-1334.
40. Z. Wei, A. S. Filatov and E. V. Dikarev, *J. Am. Chem. Soc.*, 2013, **135**, 12216-12219.
41. X. B. Li, G. Musie and D. R. Powell, *Acta Crystallogr E*, 2003, **59**, M717-M718.
42. H. X. Yang, C. J. Nie, Y. G. Shi, H. C. Yu, S. Ding, Y. L. Liu, D. Wu, N. L. Wang and J. Q. Li, *Solid State Commun.*, 2005, **134**, 403-408.
43. S. Hwang, Y. Lee, E. Jo, K. Y. Chung, W. Choi, S. M. Kim and W. Chang, *ACS Appl. Mater. Interfaces*, 2017, **9**, 18883-18888.
44. F. T. Huang, M. W. Chu, G. J. Shu, H. S. Sheu, C. H. Chen, L. K. Liu, P. A. Lee and F. C. Chou, *Phys Rev B*, 2009, **79**, 014413.
45. Q. Huang, M. L. Foo, J. W. Lynn, H. W. Zandbergen, G. Lawes, Y. Y. Wang, B. H. Toby, A. P. Ramirez, N. P. Ong and R. J. Cava, *Journal of Physics-Condensed Matter*, 2004, **16**, 5803-5814.
46. T. J. Willis, D. G. Porter, D. J. Voneshen, S. Uthayakumar, F. Demmel, M. J. Gutmann, M. Roger, K. Refson and J. P. Goff, *Sci Rep*, 2018, **8**, 3210.
47. M. Blangero, D. Carlier, M. Pollet, J. Darriet, C. Delmas and J. P. Doumerc, *Phys Rev B*, 2008, **77**, 184116.
48. L. W. Shacklette, T. R. Jow and L. Townsend, *J. Electrochem. Soc.*, 1988, **135**, 2669-2674.
49. M. G. Lazarraga, L. Pascual, H. Gadjov, D. Kovacheva, K. Petrov, J. M. Amarilla, R. M. Rojas, M. A. Martin-Luengo and J. M. Rojo, *J. Mater. Chem.*, 2004, **14**, 1640-1647.
50. L. Zhou, D. Y. Zhao and X. W. Lou, *Angew. Chem. Int. Ed.*, 2012, **51**, 239-241.

Graphic Abstract

The heterobimetallic single-source precursor $NaCo(acac)_3$ featured 1D chain structure, was firstly designed to achieve the layered oxide P2-Na_xCoO_2 with superior rate capability for Na-ion batteries (SIBs). It opens a new avenue to synthesize high-performance layered oxide cathode materials for SIBs.